



## ELASTOPLASTIC ANALYSIS OF REINFORCED 2D DOMAINS

### **Humberto B Coda**

São Carlos School of Engineering, University of São Paulo, Av. Carlos Botelho 1465, 13560-250 São Carlos, Brazil, E-mail: hbcoda@sc.usp.br

### **Wilson S Venturini**

São Carlos School of Eng., University of São Paulo, Av. Carlos Botelho 1465, 13560-250 São Carlos, Brazil, E-mail: venturin@sc.usp.br

***Abstract:** In this paper a two-dimensional elastoplastic boundary element formulation is presented to analyse composite domains. The non-linear effects are assumed to develop only over the matrix material. In order to take into account the non-linear effects, the usual procedure based on the initial stress technique is adopted. The final non-linear system of equations is analysed by using explicit and implicit techniques. The internal values are approximated over isoparametric cells to perform the required domain integrals. The reinforcement used to define the composite is given by introducing internal bars, approximated by finite elements. The bar stiffnesses are then transferred to the 2D algebraic equations using the inclusion technique. The contact between matrix and the reinforced material is assumed without relative displacements, i.e. no debonding takes place. Numerical examples are shown to illustrate the accuracy and the stability of the developed algorithm, comparing the final numerical results with experimental ones.*

**Key words:** Boundary elements, Non-linear analysis, and Composite domains

## **1. INTRODUCTION**

The boundary element method (BEM) has already proved to be a powerful tool to solve elastic and inelastic problems in the continuum mechanics context (Brebbia et al., 1984; Telles, 1983; Coda & Venturini, 1999). More recently, the couplings of Finite Element Method (FEM) and BEM have been proposed to solve specific problems where both techniques can be employed together taking the advantages of their best characteristics (Coda & Venturini, 1995; Luco & Barros, 1994).

In this paper, we choose to treat composite materials, more specifically elastic fibbers (FEM) embedded into elastoplastic matrices (BEM). The advantage of employing BEM to model the matrix material is the higher accuracy observed when this technique is used to evaluate internal stresses (or strain). On the other hand, the thin fibbers can be modelled by a very simple and accurate a truss bar finite element model.

Some aspects regarding the integration techniques for non-linear BEM are mentioned, as well as the way followed to establish the coupling technique. An example is then selected to demonstrate the accuracy and applicability of the developed numerical algorithm.

## 2. BEM NON-LINEAR FORMULATION

The well-known initial stress concept is adopted here as the starting point to derive the non-linear BEM formulation. Thus, the boundary integral representations for displacements and strains at internal points are given by:

$$C_{ik}(S)u_k(S) = \int_{\Gamma} p_k(Q)u_{ik}^*(S, Q)d\Gamma(Q) - \int_{\Gamma} u_k(Q)p_{ik}^*(S, Q)d\Gamma(Q) + \int_{\Omega} b_k(q)u_{ik}^*(S, q)d\Omega(q) + \int_{\Omega} \sigma_{\ell k}^p(q)\varepsilon_{\ell ki}^*(S, q)d\Omega(q) \quad (1)$$

$$\varepsilon_{ij}^*(s) = \int_{\Gamma} p_k(Q)\hat{\varepsilon}_{ikj}^*(S, Q)d\Gamma(Q) - \int_{\Gamma} u_k(Q)\hat{p}_{ikj}^*(S, Q)d\Gamma(Q) + \int_{\Omega} b_k(q)\hat{\varepsilon}_{ikj}^*(S, q)d\Omega(q) + \int_{\Omega} \sigma_{\ell k}^p(q)\hat{\varepsilon}_{\ell kij}^*(S, q)d\Omega(q) - \sigma_{jk}^p(s) \int_{\Gamma'} \frac{(\varepsilon_{\ell ki}^* + \varepsilon_{\ell kj}^*)}{2} d\Gamma' \quad (2)$$

where the following values must be specified:

$u_k$  - Displacement in the k direction.

$p_k$  - Traction in the k direction

$u_{ik}^*$  - Displacement in the k direction due to a unit concentrated load applied in i direction at any source point s of an infinite domain.

$b_k$  - Body force in the k direction.

$C_{ik}$  - Free term dependent upon the boundary geometry at the source point s.

Q or q - Field point either taken along the boundary or inside the domain.

S or s - Source point taken along the boundary, inside or outside the domain.

$\varepsilon_{ij}(s)$  - Strain component at an internal source point s.

$p_{ik}^*$ ,  $\hat{\varepsilon}_{ijk}^*(S, Q)$ ,  $\hat{p}_{iik}^*(S, Q)$ ,  $\hat{\varepsilon}_{ijk\ell}^*(S, q)$  and  $\hat{\varepsilon}_{ijk}^*(S, q)$  - tractions, strains and other values derived from the displacement field  $u_{ik}^*$ .

$\Gamma'$  - Unit circle around the source point.

In order to find the algebraic equations of BEM, equations (1) and (2) must be discretized by assuming boundary and internal value approximations. We have adopted quadratic isoparametric elements along the boundary to approach displacements and tractions, while quadratic quadrilateral isoparametric cells were adopted to approximate the initial stress field over the domain. By taking into account those approximations, the following algebraic equations are obtained:

$$HU = Bf + GP + Q\sigma^0 + Q\sigma^p \quad (3)$$

$$\varepsilon = B'f + G'P - H'U + Q'\sigma^0 + Q'\sigma^p \quad (4)$$

in which, vectors and matrices are the well-known ones defined for BEM formulations.

As  $\sigma^p$  is given in terms of  $\varepsilon$ , equation (4) is non-linear requiring appropriate schemes to be treated. Equations (3) and (4) depends on each other and therefore must be solved together.

This procedure is however simple, equation (3) can be easily replaced into (4) reducing the degrees of freedom required for this non-linear analysis. Thus, the solution can start by imposing boundary conditions to both equations, which does not reduce the degrees of freedom. This step is made, as usual in BEM formulations, by interchanging columns of matrices  $\mathbf{H}$  and  $\mathbf{G}$ , and  $\mathbf{H}'$  and  $\mathbf{G}'$  as well leading to:

$$\mathbf{A}\mathbf{Y} = \mathbf{F} + \mathbf{Q}\sigma^p \quad (5)$$

$$\boldsymbol{\varepsilon} = \mathbf{F}' - \mathbf{A}'\mathbf{Y} + \mathbf{S}\sigma^p \quad (6)$$

where  $\mathbf{A}$  and  $\mathbf{A}'$  contain the coefficients due to the unknown boundary values,  $\mathbf{F}$  and  $\mathbf{F}'$  are independent vectors due to prescribed boundary conditions and body forces and  $\mathbf{Y}$  is the vector containing boundary displacement and traction unknowns.

Solving equation (5) in terms of  $\mathbf{Y}$ , one has:

$$\mathbf{Y} = \mathbf{A}^{-1}\mathbf{F} + \mathbf{A}^{-1}\mathbf{Q}\sigma^p \quad (7)$$

Replacing equation (7) into equation (6) gives:

$$\boldsymbol{\varepsilon} = \boldsymbol{\varepsilon}^e + \bar{\mathbf{S}}\sigma^p \quad (8)$$

where

$$\boldsymbol{\varepsilon}^e = \mathbf{F}' - \mathbf{A}'\mathbf{A}^{-1}\mathbf{F} \quad (9a)$$

$$\bar{\mathbf{S}} = \mathbf{S} - \mathbf{A}'\mathbf{A}^{-1}\mathbf{Q} \quad (9b)$$

Equation (8) is the system of algebraic equations that must be solved to compute non-linear solutions of elasto-plastic bodies.

Before describing the fibber finite element model to couple with the BEM relations, it is recommended to describe the line load element used to represent the fibber reaction inside the continuum.

The line load due to the embedded fibbers, shown in Figure 1, is given by a couple of lines (it could also be approximated by a single line) along which the contact forces will be transferred between the steel and matrix materials. Inside the matrix material, represented by the BEM equations, those lines of loads are treated similarly to tractions over the boundary; therefore, they are approximated by using nodal values and shape functions. On the other hand, displacements are exactly represented by integral equations, although computed only at particular points defined along the fibber skeleton lines. One can compute a matrix similar to  $\mathbf{G}$  to represent the contact force influences.

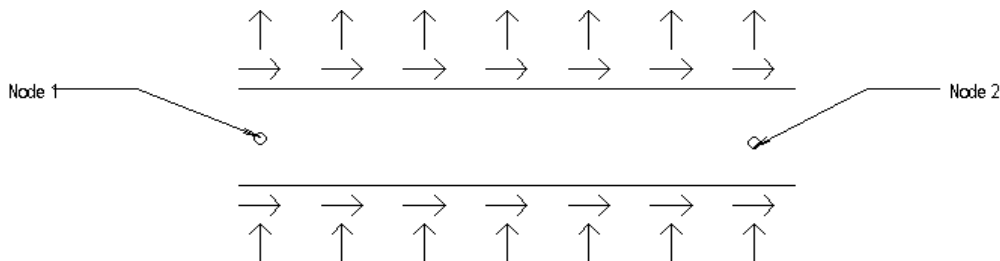


Figure 1. Internal load lines. Collocation points along the bar central line.

The same scheme used to couple steel bars with the solid along internal lines can be extended to consider this coupling along the solid boundary. One has only to write the proper expressions to take into account that particular coupling.

### 3. FIBBER FEM MODEL

As it was already said, the simple truss bar finite element is adopted here to model internal elastic fibbers. For a better comprehension, let us review quickly this formulation, starting by the virtual work principle from which a non-usual finite element approach can be derived.

$$\int_{\Omega} \bar{\epsilon} \sigma d\Omega = \int_{\Gamma} \bar{u} p d\Gamma + \sum \bar{u}_i F_i \quad (10)$$

Usually from the first term of the right hand side of equation (10), one obtains the equivalent nodal force vector. If the traction surfaces  $p$  are unknown and approximated, this term leads to the lumping matrix named here  $\mathbf{G}$  as well. By neglecting the concentrated forces, the second term in equation (10), one can write the following set of algebraic equations:

$$\mathbf{K} \mathbf{U}_{\text{FEM}} = \mathbf{G}_{\text{FEM}} \mathbf{P}_{\text{FEM}} \quad (11)$$

where matrix  $\mathbf{G}_{\text{FEM}}$  is easily derived and given by:

$$\mathbf{G}_{\text{FEM}} = \begin{bmatrix} \frac{L}{3} \cos^2 \theta & \frac{L}{3} \cos \theta \sin \theta & \frac{L}{6} \cos^2 \theta & \frac{L}{6} \cos \theta \sin \theta \\ \frac{L}{3} \cos \theta \sin \theta & \frac{L}{3} \sin^2 \theta & \frac{L}{6} \cos \theta \sin \theta & \frac{L}{6} \sin^2 \theta \\ \frac{L}{6} \cos^2 \theta & \frac{L}{6} \cos \theta \sin \theta & \frac{L}{3} \cos^2 \theta & \frac{L}{3} \cos \theta \sin \theta \\ \frac{L}{6} \cos \theta \sin \theta & \frac{L}{6} \sin^2 \theta & \frac{L}{3} \cos \theta \sin \theta & \frac{L}{3} \sin^2 \theta \end{bmatrix} \quad (12)$$

with  $\theta$  being the angle between the local direction  $\bar{\mathbf{x}}$  and the corresponding global direction; the subscript "FEM" denotes finite element nodes.

### 4. BEM/FEM COUPLING

The coupling treated here is concerned with the combination of two systems of algebraic equations: one representing a 2D body obtained by using BEM and another representing the entirely embedded bar system governed by FEM algebraic relations.

The equilibrium and geometrical compatibility conditions have to be assumed along the contact and can be represented by:

$$\mathbf{P}^{\text{C}} = -\mathbf{P}^{\text{FEM}} \quad (13)$$

$$\mathbf{U}^{\text{C}} = \mathbf{U}^{\text{FEM}} \quad (14)$$

where the superscript "C" denotes boundary element nodes connected to the finite element domain.

From these assumptions, equation (11) can be modified to give:

$$\mathbf{P}^{\text{FEM}} = \mathbf{G}_{\text{FEM}}^{-1} \mathbf{K} \mathbf{U}^{\text{FEM}} \quad (15)$$

One can substitute equation (15) into equations (3) and (4), taking into account equations (13) and (14) to obtain:

$$\begin{bmatrix} \mathbf{H}^d & \mathbf{H}^c \end{bmatrix} \begin{Bmatrix} \mathbf{U}^d \\ \mathbf{U}^c \end{Bmatrix} = \mathbf{G}^d \mathbf{P}^d + \mathbf{G}_c [-\mathbf{G}_{\text{FEM}}^{-1} \mathbf{K} \mathbf{U}_c] + \mathbf{Q} \sigma^p \quad (16)$$

$$\boldsymbol{\varepsilon} = \mathbf{G}'^d \mathbf{P}^d + \mathbf{G}'_c [-\mathbf{G}_{\text{FEM}}^{-1} \mathbf{K} \mathbf{U}_c] - \begin{bmatrix} \mathbf{H}'^d & \mathbf{H}'^c \end{bmatrix} \begin{Bmatrix} \mathbf{U}^d \\ \mathbf{U}^c \end{Bmatrix} + \mathbf{S} \sigma^p \quad (17)$$

where "d" stands for disconnected BEM nodes.

Rearranging equations (16) and equation (17) one finds:

$$\begin{bmatrix} \mathbf{H}^d & \bar{\mathbf{H}}^c \end{bmatrix} \begin{Bmatrix} \mathbf{U}^d \\ \mathbf{U}^c \end{Bmatrix} = \mathbf{G}^d \mathbf{P}^d + \mathbf{Q} \sigma^p \quad (18)$$

$$\boldsymbol{\varepsilon} = \mathbf{G}'^d \mathbf{P}^d - \begin{bmatrix} \mathbf{H}'^d & \bar{\mathbf{H}}'^c \end{bmatrix} \begin{Bmatrix} \mathbf{U}^d \\ \mathbf{U}^c \end{Bmatrix} + \mathbf{S} \sigma^p \quad (19)$$

where

$$\bar{\mathbf{H}}_c = \mathbf{H}_c + \mathbf{G}_c \mathbf{G}_{\text{FEM}}^{-1} \mathbf{K} \quad (20a)$$

$$\bar{\mathbf{H}}'_c = \mathbf{H}'_c + \mathbf{G}'_c \mathbf{G}_{\text{FEM}}^{-1} \mathbf{K} \quad (20b)$$

Writing equations (18) and (19) into a more compact form we have:

$$\mathbf{H}^* \mathbf{U} = \mathbf{G} \mathbf{P} + \mathbf{Q} \sigma^p \quad (21)$$

$$\boldsymbol{\varepsilon} = \mathbf{G}' \mathbf{P} - \mathbf{H}'^* \mathbf{U} + \mathbf{S} \sigma^p \quad (22)$$

Equations (21) and (22) represent the reinforced body algebraic equations. They exhibit the usual form of the BEM algebraic representation. Thus, one can follow the usual procedure, given by equations (9), to deal with reinforced non-linear problems.

## 5. SOLUTION PROCEDURE

In order to solve the non-linear system of equations (9), an incremental scheme must be followed. This can be obtained by expanding equation (9), as follows:

$$\boldsymbol{\varepsilon}_s + \Delta \boldsymbol{\varepsilon}_{s+1} = \boldsymbol{\varepsilon}_s^e + \Delta \boldsymbol{\varepsilon}_{s+1}^e + (\boldsymbol{\sigma}_s^p + \frac{\partial \boldsymbol{\sigma}^p}{\partial \boldsymbol{\varepsilon}} \Delta \boldsymbol{\varepsilon}_{s+1}) \quad (23)$$

where s is a defined load level.

The term  $\frac{\partial \boldsymbol{\sigma}^p}{\partial \boldsymbol{\varepsilon}}$  is a well-known value for elastoplastic analysis, relating strain and elasto-plastic stress variations, which is usually referred as  $\mathbf{C}_p$  (Simo & Taylor, 1985). Thus, equation (23) becomes,

$$(\mathbf{I} - \mathbf{S} \mathbf{C}_p) \Delta \boldsymbol{\varepsilon}_{s+1} = (\boldsymbol{\varepsilon}_s^e + \mathbf{S} \boldsymbol{\sigma}_s^p - \boldsymbol{\varepsilon}_s) + \Delta \boldsymbol{\varepsilon}_{s+1}^e \quad (24)$$

or

$$(\mathbf{I} - \mathbf{S} \mathbf{C}_p) \Delta \boldsymbol{\varepsilon}_{s+1} = \boldsymbol{\varphi}_s + \Delta \boldsymbol{\varepsilon}_{s+1}^e \quad (25)$$

For an approximate case, the first term on the right hand side of equation (24) is a trial correction, and computed as a residual from the previous time step. From equation (24), several integration schemes can be followed to solve a non-linear problem. The simplest one is known as the explicit scheme and has been employed together with BEM formulations many times (Brebbia et al., 1984). The second one, named here the tangent explicit algorithm, is described by the following steps:

a<sub>1</sub>) Computing the strain increment

$$\Delta \boldsymbol{\varepsilon}_{s+1}^1 = \boldsymbol{\varphi}_s + \Delta \boldsymbol{\varepsilon}_{s+1}^e \quad (26)$$

a<sub>2</sub>) Elastic stress prevision

$$\Delta \boldsymbol{\sigma}_{s+1}^1 = \mathbf{C} \Delta \boldsymbol{\varepsilon}_{s+1}^1 \quad (27)$$

or

$$\boldsymbol{\sigma}_{s+1}^1 = \boldsymbol{\sigma}_s + \Delta \boldsymbol{\sigma}_{s+1}^1 \quad (28)$$

a<sub>3</sub>) Yielding test. If yielding is not reached go to a<sub>1</sub> making s=s+1 to start a new increment with  $\boldsymbol{\varphi}_{s+1} = 0$ . Otherwise,

$$\Delta \boldsymbol{\sigma}_{s+1}^1 = \Delta \boldsymbol{\sigma}_{s+1}^1 - \Delta \boldsymbol{\sigma}_{s+1}^p \quad (29)$$

$$\Delta \boldsymbol{\varepsilon}_{s+1}^p = \boldsymbol{\varepsilon}_s^p + \Delta \boldsymbol{\varepsilon}_{s+1}^{1p} \quad (30)$$

Storage the value  $\mathbf{C}_p^1$ .

a<sub>4</sub>) Correction phase.

$$\Delta \boldsymbol{\varepsilon}_{s+1}^{2p} = (\mathbf{I} - \mathbf{S} \mathbf{C}_p^1) \Delta \boldsymbol{\sigma}_{s+1}^{1p} \quad (31)$$

The increment  $\Delta \boldsymbol{\sigma}_{s+1}^{1p}$  represents the error of the whole process described in equation (24). Go to item a<sub>2</sub>.

a<sub>5</sub>) Convergence test.

$$\left| \frac{\Delta \boldsymbol{\sigma}_{s+1}^{np} - \Delta \boldsymbol{\sigma}_{s+1}^{n-1p}}{\Delta \boldsymbol{\sigma}_{s+1}^{np}} \right| < \text{tol} \quad (32)$$

Then compute

$$\boldsymbol{\varphi}_{s+1} = \boldsymbol{\varepsilon}_{s+1}^e + \mathbf{S} \boldsymbol{\sigma}_{s+1}^p - \boldsymbol{\varepsilon}_{s+1} \quad (33)$$

Go to a<sub>1</sub> to start a new increment.

The second possible non-linear algorithm procedure is the implicit one (see Bonnet & Mukerjee, 1996 and also Fudoli et al., 1999). Equation (24) is employed in its original form giving the tangent operator  $\mathbf{C}_p(\Delta \boldsymbol{\varepsilon}_{s+1})$ . For von Mises yielding criterion this tangent operator is given in a closed form, allowing therefore the direct application of equation (24). For other

criteria with more complex representation in the stress space, an iterative process must be provided to achieve implicitly the operator  $C_p(\Delta\epsilon_{s+1})$ .

## 6. EXAMPLE

The example chosen to illustrate the non-linear reinforced BEM model compares values achieved by using the numerical procedure with experimental results. This example is appropriate to show the stability of the numerical technique and also to emphasise that the non-linear criterion chosen can represent the reinforced concrete beam behaviour.

The analysed reinforced concrete beam is shown in Figure 1, where its sizes are given together with the embedded longitudinal and shear reinforcements. The load  $F$ , also shown in Figure 1, is gradually applied starting from zero to its maximum value  $F = 13.5 \times 10^5 \text{ kg.cm/s}^2$ . The adopted discretization is displayed in Figure 2, in which boundary and steel bars elements are displayed. The material properties assumed for this analysis are the same ones evaluated at our laboratory by Martinelli & Takeya, (1974):  $E_{co} = 2.0 \times 10^8 \text{ kg/(cm.s}^2)$ ,  $E_{cs} = 1.96 \times 10^9 \text{ kg/(cm.s}^2)$ ,  $\nu = 0.2$ ,  $f_c = 3.92 \times 10^5 \text{ kg/(cm.s}^2)$  and  $f_t = 0.3 \times 10^5 \text{ kg/(cm.s}^2)$ . The concrete Young's modulus adopted was computed by finding the average value between the initial one and the value corresponding to the maximum compression strain, i.e. when the strain reached  $2/1000$  in compression. For this case, we have chosen the Drucker Prager yielding surface to represent the concrete matrix behaviour, while the steel bars were assumed to be elastic. The criterion parameters,  $c = 5.44 \times 10^4 \text{ kg/(cm.s}^2)$  and  $\phi = 1.03 \text{ rad}$ , were established from the experimental values given above. No relative displacement was assumed between steel bars and concrete matrix.

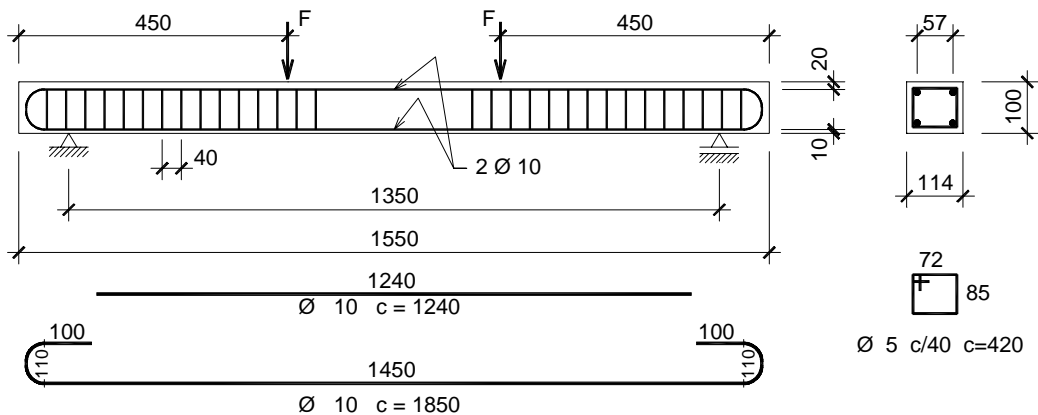


Figure 1: Reinforced concrete beam, geometry and loading (values in mm)

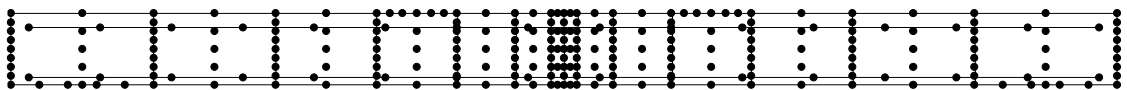


Figure 2: Boundary and steel bar discretizations.

The numerical displacements computed at the central node are compared with experimental values in Figure 3. Although, the criterion parameters have been defined directly from particular samples collected from the concrete mass prepared to build the beam, the final

results compare well with the numerical solution. It is possible to see that some differences between the experimental and numerical curves appeared after the cracking point. The beam experimented in the laboratory shows a more abrupt stiffness reduction after cracking. The adopted model for the numerical analysis does not show this reduction. In average, the chosen model can represent well the overall beam behaviour. The evolution of the internal effective stresses is given in Figure 4, for some selected load levels. Although no comparison with other numerical model has been made, the results exhibit an expected distribution of effective stresses over the beam. The same conclusion can be made on the longitudinal and shear stress distributions illustrated in Figures 5 and 6, respectively. It is also important to verify the shear stresses along the contact to confirm the no debonding assumption (Figure 7). Practically, the same results have been obtained following the two integration schemes discussed in this paper to treat the non-linear system of equations.

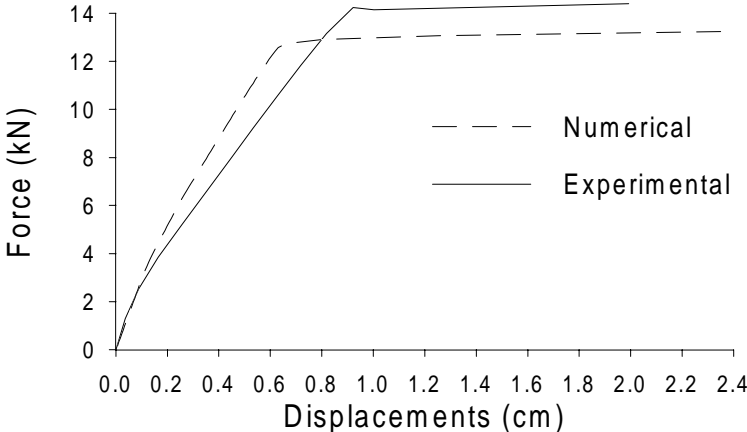


Figure 3: Loading versus central displacement

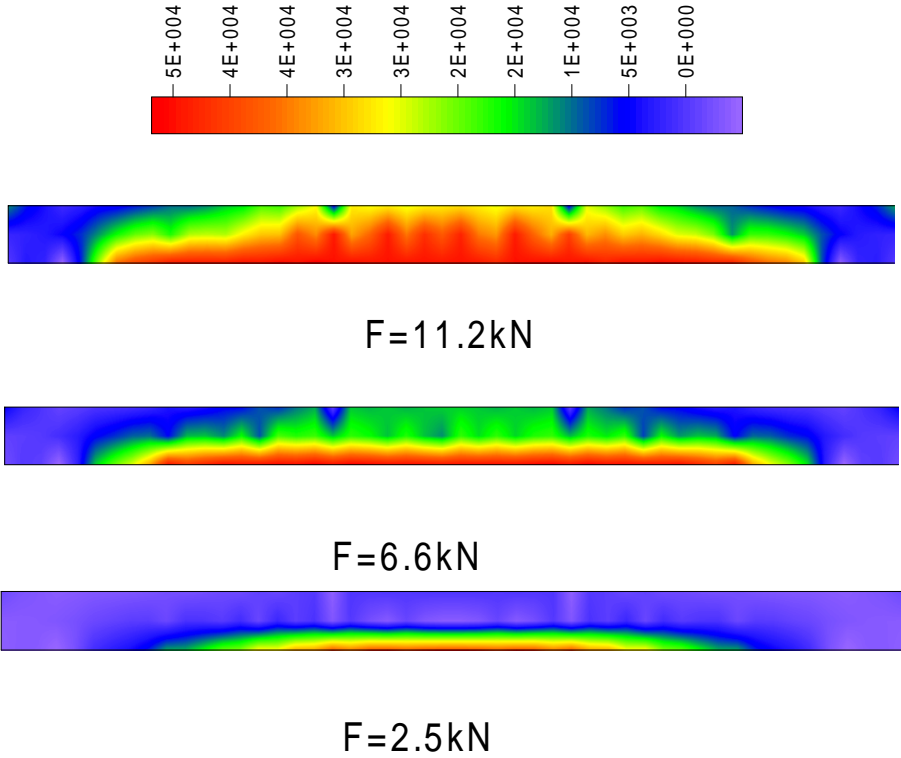


Figure 4: Internal effective stress level for selected loads

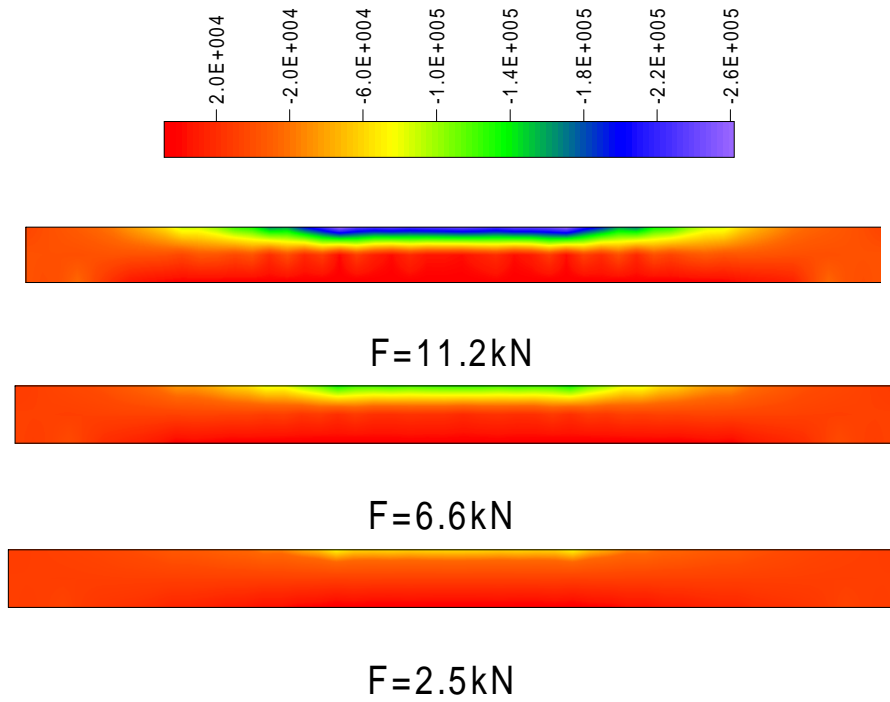


Figure 5: Normal stress distribution (horizontal component)

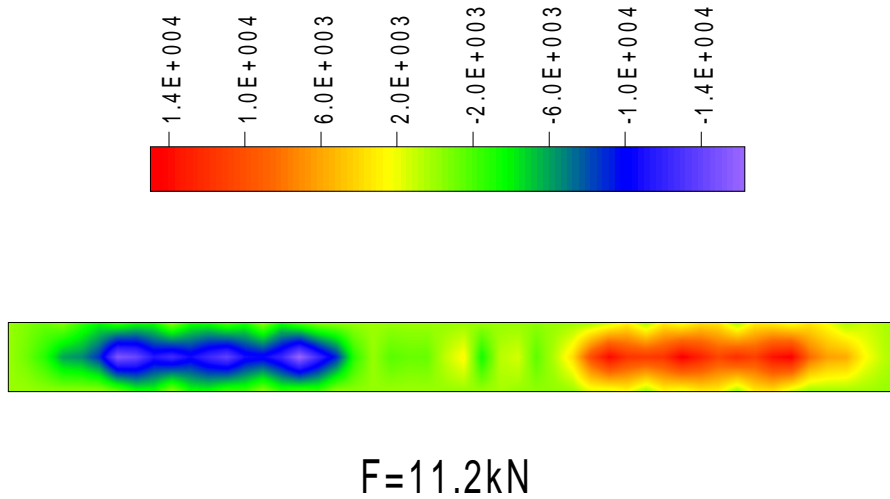


Figure 6: Shear stress distribution for selected loads

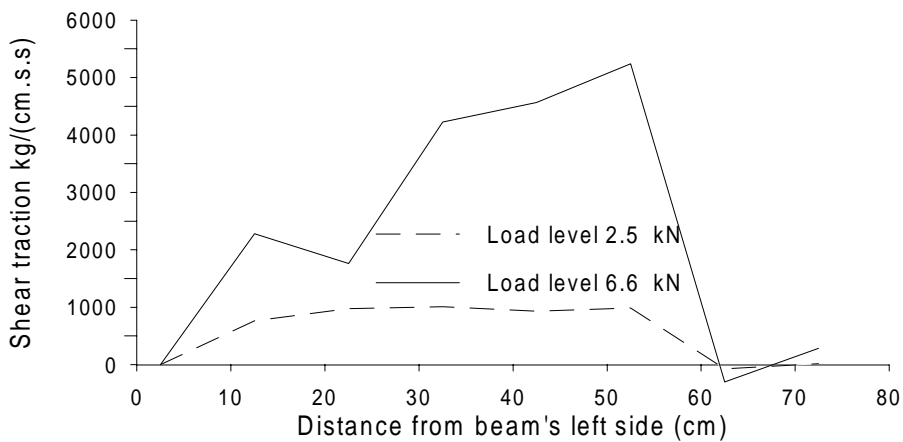


Figure 7: Contact shear traction between concrete and steel

## 7. CONCLUSION

A particular model to analyse composite material with emphasis to non-linearities over the matrix material has been proposed. The model was developed for any kind of internal fibers combined with elasto-plastic material matrix only. The boundary element method was used to model the non-linear domain, while simple truss bar finite elements have been adopted to simulate the fibers. Two procedures used to integrate the non-linear relations have been tested and confirmed the good performance of BEM for this kind of problems. The model was taken to analyse a reinforced concrete beam and the main results compared with the experimental values.

## REFERENCES

- Bonnet, M. & Mukherjee, S., 1996, Implicit BEM formulation for usual and sensitivity problems in elasto-plasticity using the consistent tangent operator concept. *Int. J. Solids Struct.*, 33, 4461-4480.
- Brebbia, C.A.; Telles, J.C.F. & Wrobel, L.C., 1984, *Boundary Element Techniques*. Springer Verlag, Berlin.
- Coda, H.B. & Venturini, W.S., 1995, Three dimensional transient BEM analysis. *Computer of Structures*, v. 56, n. 5, p.751-768, Pergamon.
- Coda, H.B. & Venturini W.S. 1999, Dynamic non-linear stress analysis by the mass matrix BEM emphasising the acceleration aspects. *Engineering Analysis with Boundary Elements*, Submitted.
- Fudoli, C.A., Venturini, W.S. & Benallal, A., 1999, Implicit and explicit elastoplastic BEM formulations applied to localization. COBEM99 – XV Brazilian Congress on Mechanical Engineering.
- Luco, J.E. & Barros, C.P., 1994, Seismic response of a cylindrical shell embedded in a layered viscoelastic half-space Part I & II. *Earthquake engineering and structural dynamics*, 23, 553-567.
- Martinelli, D.A.O. & Takeya, T., 1974, *Ruína das ligações laje-pilar nas bordas de lajes-cogumelo*, Escola de Engenharia de São Carlos, Relatório FAPESP (in Portuguese).
- Simo, J.C. & Taylor, R.L., 1985, Consistent tangent operators for rate-independent elastoplasticity. *Comp. Meth. Appl. Mech. Engng*, 48, 101-118.
- Telles, J.C.F, (1983), *Boundary element method applied to inelastic problems*. Lecture Notes in Engineering, 1, Springer-Verlag, Berlin and Heidelberg.